

On MHD jet production in the collapsing and rotating envelope

Daniel Proga,¹

¹ *Princeton University Observatory, Peyton Hall, Princeton, NJ 08544.e-mail: dproga@astro.princeton.edu*

ABSTRACT

We present results from axisymmetric, time-dependent hydrodynamical (HD) and magnetohydrodynamical (MHD) simulations of a gaseous envelope collapsing onto a black hole (BH). We consider gas with so small angular momentum that after an initial transient, the flow in the HD case, accretes directly onto a BH without forming a rotationally support torus. However, in the MHD case even with a very weak initial magnetic field, the flow settles into a configuration with four components: (i) an equatorial inflow, (ii) a bipolar outflow, (iii) polar funnel outflow, and (iv) polar funnel inflow. We focus our analysis on the second flow component of the MHD flow which represents a simple yet robust example of a well-organized inflow/outflow solution to the problem of MHD jet formation. The jet is heavy, highly magnetized, and driven by magnetic and centrifugal forces. A significant fraction of the total energy in the jet is carried out by a large scale magnetic field. We review previous simulations, where specific angular momentum was higher than that assumed here, and conclude that our bipolar outflow develops for a wide range of the properties of the flow near the equator and near the poles. Future work on such a simple inflow/outflow solution will help to pinpoint the key elements of real jets/outflows as well as help to interpret much more complex simulations aimed at studying jet formation and collapse of magnetized envelopes.

Subject headings: accretion, accretion disks – methods: numerical – MHD – stars: winds, outflows

1. Introduction

The common occurrence and importance of astrophysical jets have stimulated many theoretical studies. Both analytic and numerical studies provide strong support for the scenario where jets are magnetohydrodynamic (MHD) in character and are associated with

an accretion disk, a rotating accretor, or both (e.g., Blandford & Payne 1982; Blandford 1990; De Villier et al. 2003). In fact, most MHD simulations of accretion flows show outflows (e.g., Uchida & Shibata 1985; Stone & Norman 1994; Hawley & Balbus 2002; De Villier et al. 2004; Mizuno et al. 2004; Kato et al. 2004; McKinney & Gammie 2004).

Here, we describe a study of the time evolution of MHD flows in the vicinity of a stationary black hole (BH). This study has been motivated by the results from our previous work (Proga & Begelman 2003b, hereafter PB03b; Proga et al 2003) which showed that large-scale magnetic fields can produce a jet from a rotationally supported accretion disk or torus and also from extremely low angular momentum gas that almost radially accretes onto a BH. This falling gas and associated outflow can be well-organized and a simple, self-consistent solution for the MHD jet problem. However, in our previous simulations and likely in some other simulations, this simple inflow/outflow is a component of a complex convolution of a rotationally supported, MHD turbulent torus, the torus corona and outflow. To articulate the basic physics that occurs in jet production, we focus on a flow with angular momentum so low that, if not for the effects of MHD, the flow would accrete directly onto a BH without forming a disk.

2. Method

To calculate the flow structure and evolution, we solve the equations of ideal MHD:

$$\frac{D\rho}{Dt} + \rho\nabla \cdot \mathbf{v} = 0, \quad (1)$$

$$\rho \frac{D\mathbf{v}}{Dt} = -\nabla P - \rho\nabla\Phi + \frac{1}{4\pi}(\nabla \times \mathbf{B}) \times \mathbf{B}, \quad (2)$$

$$\rho \frac{D}{Dt} \left(\frac{e}{\rho} \right) = -P\nabla \cdot \mathbf{v}, \quad (3)$$

$$\frac{\partial \mathbf{B}}{\partial t} = \nabla \times (\mathbf{v} \times \mathbf{B}), \quad (4)$$

where ρ is the mass density, P is the total gas pressure plus radiation pressure, \mathbf{v} is the fluid velocity, e is the internal energy density, Φ is the gravitational potential, and \mathbf{B} is the magnetic field vector. We adopt an adiabatic equation of state $P = (\gamma - 1)e$ and consider models with $\gamma = 5/3$.

We perform simulations using the pseudo-Newtonian potential of the central mass $\Phi_{PW} = GM/(r - R_S)$, where $R_S = 2GM/c^2$ is the Schwarzschild radius, introduced by Paczyński & Wiita (1980). This potential approximates general relativistic effects in the inner regions, for a nonrotating black hole. In particular, the Paczyński–Wiita potential reproduces the last stable circular orbit at $r = 3R_S$ as well as the marginally bound orbit at $r = 2R_S$.

Our calculations are performed in spherical polar coordinates (r, θ, ϕ) . We assume axial symmetry about the rotational axis of the accretion flow ($\theta = 0^\circ$ and 180°). The computational domain occupies the radial range $r_i = 1.5 R_S \leq r \leq r_o = 1200 R_S$, and the angular range $0^\circ \leq \theta \leq 180^\circ$. The $r - \theta$ domain is discretized on a non-uniform grid as in PB03b.

Our calculations use the ZEUS-2D code described by Stone & Norman (1992a,b). We adopt PB03b’s boundary and initial conditions but we make two modifications to the initial conditions (see below). An important element of the initial conditions is that the rotating gas has constant specific angular momentum, l , and is confined in a wedge near the equator between $\theta = 90^\circ - \theta_0$ and $\theta = 90^\circ + \theta_0$. The wedge of the rotating gas is truncated at the radius, $r(v_r = c_\infty)$ defined as the radius where the initial radial velocity (as predicted by modified Bondi velocity law, see Proga & Begelman 2003a, hereafter PB03a) equals the sound speed at infinity, c_∞ .

The two modifications of the PB03b initial conditions are: (i) we set the initial conditions exactly as in PB03b and then reduce the density and internal energy by a factor of 100 in the part of the computational domain where $v_\phi = 0$ (outside the rotating wedge) and (ii) we consider two field geometries: a purely radial magnetic field as in PB03b and a vertical magnetic field defined by the potential $\mathbf{A} = (A_r = 0, A_\theta = 0, A_\phi = Ar \sin \theta)$. For $r \sin \theta > r(v_r = c_\infty)$, we scale the magnitude of the magnetic field using a parameter, $\beta_o \equiv 8\pi P_B(r_o)/B^2$ defined as the plasma parameter $\beta \equiv 8\pi P/B^2$ at r_o , so that $A = (2\pi P_B(r_o)/\beta_o)^{1/2}$ (where P_B is the gas pressure associated with the Bondi solution at r_o). For $r \sin \theta < r(v_r = c_\infty)$, we set the constant A to a very small value.

We introduce these two modifications to reduce the flow complexity. In particular, we want the rotating flow to be dominant and we want to follow the evolution of the rotating flow with as little interference as possible from other flow components.

We choose the following units: $r_0 = R_S$, $t_0 = 4\pi(R_S^3/2GM)^{1/2}$, $v_0 = c$, $B_0 = (4\pi\rho_\infty c^2)^{1/2}$, $\rho_0 = \rho_\infty$ (the density at infinity for a classic Bondi flow). The force is in units of $f_0 = c^4/4GM$ and the specific angular momentum is in units of $l_0 = 2R_S c$.

3. Results

To simulate a simple inflow/outflow solution we must appropriately set the model parameters. Our initial conditions help to promote the dominance the rotating flow and reduce effects of the non-rotating flow. The importance of the non-rotating flow depends not only on the initial conditions but also on the minimum value of the density allowed in the simulations, the so-called density floor, ρ_f . We set $\rho_f = (1/r)^{1/2}$. For comparison, the maximum density at small radii achieved during the simulation is about 10^4 . To aid the rotating flow in reaching an organized solution we set l smaller than the critical angular momentum, $2R_{sc}$. [Otherwise the rotating gas will form a rotationally supported torus which becomes turbulent and generates a magnetized complex corona and outflow (e.g., PB03b).] Here we describe results from the simulations with $l = 0.8$. We set $\theta_0 = 56^\circ$ (as in a fiducial model in PB03b).

For our choice of l , the flow near the equator is sub-Keplerian at all radii and will likely stay sub-Keplerian during the evolution with appreciable radial velocity (i.e., the equatorial flow may continue to accrete supersonically). This feature distinguishes our simulations from many previous ones where the focus was on the outflows from rotationally supported disks or torii. Our main focus is on formation of an outflow from nearly radially falling gas away from the equator.

We have performed numerous simulations varying the magnitude and geometry of the magnetic field, the specific angular momentum, the numerical resolution and the density floor. Here we present results from two models: model A without a magnetic field and model B for which $\beta_o = 10^3$ and the initial magnetic field is vertical. Model A is a reference model which illustrates the flow pattern when accretion proceeds directly whereas model B illustrates the dynamics and properties of simplest accretion flow which generates outflow without formation of rotationally supported disk and without development of magnetorotational instability.

In the early phase of the evolution, when the flow relaxes from the initial conditions, both models show the same behaviour. First, the gas near the equator falls in nearly radially onto a BH. However, the rotating gas closer to the poles diverges away from the equator because of a lack of pressure equilibrium in the θ direction due to the density and internal energy difference between the equatorial wedge and the polar region. The flow at small radii becomes gradually radial, with the density decreasing between the equator and the poles. After this early phase, the evolution of the two models proceeds differently. In particular, the flow in model A settles down into a steady state of direct accretion whereas in model B an outflow as well as a direct accretion flow form.

Figure 1 presents the flow pattern for model A at small radii at $t = 3550$. The figure

shows the density map overplotted with the direction of the poloidal velocity. The flow has two components: (i) an equatorial inflow and (ii) a polar funnel inflow. The equatorial inflow has non-zero l but its circularization radius is inside the last stable orbit therefore direct accretion occurs. The polar funnel inflow has zero l . The density contrast between the two components is due to the fact that at the outer boundary and for the initial conditions the density of the non rotating gas is smaller than the density of the rotating gas by a factor of 100. At $t = 500$, the mass accretion rate, $\dot{M}_a = 0.08$ in units of the Bondi rate (\dot{M}_B) and then gradually increases. At the end of the simulation, $t = 3550$, $\dot{M}_a = 0.123$ and still continues to grow but very slowly. We estimate that \dot{M}_a will saturate at the level of ≈ 0.125 . We stress that there is no indication of an outflow in model A. This contrasts with the MHD counterpart of this model.

In model B, the establishment of the equatorial inflow is soon (at $t > 715$) followed by a development of a bipolar outflow from the 'shoulders' of the inflowing gas. At first, the outflow is confined to a very narrow range of θ but with time this range increases. In particular, at $t=5700$, the outflow is at $26^\circ \lesssim \theta \lesssim 48^\circ$ and $132^\circ \lesssim \theta \lesssim 154^\circ$ at $r = 20$. In other words, we observe that with time the boundary between the equatorial inflow and the bipolar outflow moves toward the equator. The mass loss rate associated with the outflow, \dot{M}_W increases with time. For example, at $t = 1500$, $\dot{M}_W = 0.0008$ while at $t = 5700$, $\dot{M}_W = 0.008$ (\dot{M}_w was measured at $r = 175$). The late time evolution of \dot{M}_a for model B differs from that for model A. Namely, for model B, $\dot{M}_a = 0.08$ at $t = 500$ and then gradually increases to 0.11 at $t = 1500$. The mass accretion rate stays at this level until $t = 5000$ and then decreases to 0.102 at $t = 5700$.

The magnetic field evolves from vertical to nearly radial. This change in the field geometry is a natural consequence of radially falling gas because the field lines are dragged in with the gas. However, even at the end of the simulation, the field did not evolve into a split monopole configuration due to the initial nonradial evolution of the flow.

Of course, the evolution of the field configuration is accompanied by the growth of the field strength. In particular, shear generates the toroidal field in the rotating flow. The toroidal field is fastest growing component of the field in the rotating gas and eventually dominates the poloidal field, $B_p = (B_r + B_\theta)^{1/2}$. Additionally, the continuously growing field becomes dynamically important (we find that an outflow forms in the regions where $\beta_\phi \equiv 8\pi P/B_\phi^2 < 1$). In the polar region, the poloidal field is dominant, $\beta_p \equiv 8\pi P/B_p^2 < 1$) whereas $\beta_\phi > 1$).

Figure 2 shows the flow pattern at small radii at $t = 5700$ for model B. The left and right panels show density and $|B_\phi|$ maps, respectively. The figure shows also the direction of the poloidal velocity and poloidal magnetic field as well as an example of a streamline.

The flow has four components: (i) a radial equatorial inflow, (ii) a bipolar outflow (the streamline shown in Fig. 2 is typical for this flow component), (iii) a polar funnel outflow, and (iv) a polar funnel inflow. The third and fourth components (we call collectively the funnel flow) are separated from the inflow/outflow solution by the centrifugal barrier. We note that the funnel outflow can be hardly distinguished from the bipolar outflow based on the direction of the poloidal velocity. Comparison of the panels of Fig. 2 reveals that across the boundary between the bipolar outflow and the funnel flow, three significant changes occur: (i) the density dramatically decreases; (ii) B_p changes suddenly direction, and (iii) B_ϕ increases. We also note that the polar funnel inflow is confined to a very narrow region along the rotational axis and its properties/dynamics are difficult to capture by our numerical approach because of the imposed density floor and gas heating by artificial viscosity. These effects can occasionally lead to production of a thermal outflow in the funnel (e.g., see the lower half of the left panel for $r \lesssim -11$ near the rotational axis). In the remaining part of the paper, we focus on the second component of the MHD flow – the inflow/outflow solution.

The relative simplicity and slow time evolution of the inflow/ outflow solution helps us to identify the forces responsible for production of the outflow from the infalling gas. For example, we have analyzed and compared all the terms in the equation of motion along various streamlines. The important force components in the radial direction are: gravity, f_g , gas pressure gradient, f_p , centrifugal force, f_c and gradient of the toroidal field pressure, f_m (the other components of the Lorentz force are negligible). In the latitudinal direction f_p , f_c and f_m determine the total force, f_t .

Figure 3 presents various fluid and magnetic field properties and the forces acting on the flow as a function of the pathlength (the pathlength is measured from $r = 14$ and $\theta = 53^\circ$) along the typical streamline for the inflow/outflow solution. To generate this plot, we assume that the solution is steady. This assumption is justified for our purposes here because the time changes in the flow occur on the scales significantly longer than the time needed for the flow element to follow the segment of the streamline we analyze.

Fig. 3a shows that the motion in the radial direction is determined in the following way: (1) the infall slows down and eventually stops due to the centrifugal force. Up to the stagnation point, the fluid specific angular momentum stays nearly constant (dash-dotted line in Fig. 3f). The centrifugal force can balance gravity, despite sub-Keplerian rotation on the equator, because f_c increases from the equator toward the poles [$f_c \propto 1/(r^3 \sin^2 \theta)$ for $l = const$]. Near the stagnation point, two significant changes occur in the force balance: (i) f_m becomes significant and is directed outward and (ii) f_c increases compared to gravity because the magnetic torque increases somewhat specific angular momentum of the fluid. The combined centrifugal and B_ϕ pressure forces overcome the combined gravity and gas

pressure (the latter is directed inwards) and accelerate the flow outward. Although $f_c > f_m$ in the outflow, f_c alone is not strong enough to accelerate the flow. Therefore, the flow is not 'flung out' by the centrifugal force as in Blandford & Payne's (1982) magnetocentrifugal wind but is much more gradually pushed by the pressure of the toroidal field (see Spruit 1996 and also below for a discussion of heavy loaded MHD winds).

Fig. 3b shows that as the infalling gas approaches the stagnation point, f_p pushes the gas away from the equator against the centrifugal force. Near the stagnation point, two significant changes occur in the force balance in the θ direction: (i) f_m changes sign and (ii) f_p increases so that it alone can 'collimate' the gas during the early phase of the outflow (this is done against not only f_c and also against f_m).

Farther downstream from the stagnation point, f_m again changes sign and becomes stronger than f_p . Thus, f_m appears to play an important role in the outflow collimation at large radii whereas f_p pushes the outflow away from the equator during the initial acceleration. However, when the θ component of f_m changes sign for the second time, B_r changes sign too (the dashed vertical lines in all panels of Fig. 3 mark the location where B_r changes sign downstream from the stagnation point). In ideal MHD, the magnetic field should be dragged in with the flow and no changes in the field orientation should occur within an organized outflow due to field freezing. However, in our solution of MHD equations using the grid based code, the change of B_r sign is due to annihilation (reconnection) of oppositely oriented fluxes (i.e., the polar funnel flux vs. the bipolar outflow flux) on the grid-spacing scale. We note this numerical limitation and focus on the properties of the bipolar outflow upstream from the point where the polar funnel flux annihilates the bipolar outflow flux.

The bipolar outflow is unbound and it is heavy loaded. To quantify the latter, we compute the so-called mass loading parameter $\mu \equiv (v_p v_\phi / v_{Ap}^2)^{1/2}$ (where $v_{Ap} \equiv (B_p^2 / 4\pi\rho)^{1/2}$ is the poloidal Alfvén speed) introduced by Spruit (1996, see also eq. 2 in Anderson et al. 2004; note a difference between the definition of μ in the two references). At the stagnation point, $\mu = 30$. Fig. 3d shows that the toroidal field is higher than the poloidal field (compare solid, dotted, and dashed lines) while Fig. 3f shows that the outflow does not corotate with its base and the outflow does not gain much of specific angular momentum (see dashed and dash-dotted lines in Fig. 3f for the angular velocity, Ω and specific angular momentum, respectively). All these flow characteristics are consistent with the high value of μ at the stagnation point (e.g., Spruit 1996).

Fig. 3e shows that the flow is super Alfvénic (dotted line). This figure also shows that the ratio between the Poynting flux and kinetic energy flux, F_P/F_K increases downstream from the stagnation point. The energy flux ratio becomes of order of unity near the location of the bipolar outflow 'merging' with the funnel flow (i.e., the location mark by the vertical

dashed line).

4. Summary and Concluding Remarks

We present results from asymmetric HD and MHD simulations of a rotating gas collapsing onto a stationary BH. We consider extreme cases where the gas rotation is so small that the circularization radius is inside the last stable orbit. Therefore one expects direct accretion of all gas without formation of a rotationally supported torus no mention of formation of an outflow. After an initial transient, the HD flow, as expected, settles into a configuration where direct accretion occurs and there is not outflow. This contrasts with the MHD flow, which even for a very weak initial magnetic field, settles into a configuration with four components: (i) a radial equatorial inflow, (ii) a bipolar outflow, (iii) polar funnel outflow, and (iv) polar funnel inflow. Our focus here is on the second, unexpected component of the MHD flow.

The bipolar outflow is driven by the magnetic and centrifugal forces. Following the streamlines of the bipolar outflow, we identify four stages of the flow motion: (i) a gravitational collapse, (ii) a gradual slow down and eventual termination of the collapse by the centrifugal force, (iii) launching of the outflow by gas pressure which redirects the flow away from the equator and by the centrifugal force which redirects the flow away from a BH in the radial direction (the latter force is enhanced owing to a magnetic torque spinning up the gas), and (iv) an acceleration by the centrifugal force and gradient of the toroidal field pressure. The outflow is highly magnetized ($\beta < 1$) and the Poynting flux carries a significant fraction of the total energy.

Despite performing the simulation for thousands of orbits at the inner radius the flow did not reach a steady state. One indication of the time evolution is that an increasingly larger fraction of the equatorial inflow turns into the bipolar outflow. Additionally, the inflow very close to the equator can start turning back, the equatorial symmetry breaks, and the flow near the equator starts to circulate. However, not all flow properties evolve with time. For example, the angular velocity profile along the equator is time steady and closely follows the $1/r$ scaling as expected for the constant l flow. Generally, the flow evolves over a very long time scale into a state where the bipolar outflow 'sandwiches' a smooth radial inflow or a complex flow near the equator (our test runs with $l = 0.5$ show that the equatorial flow can remain a smooth inflow for as long as the simulations). We have observed a similar bipolar outflow in almost all of our simulations performed recently or performed in PB03b and Proga et al. (2003). Our inflow/outflow solution resembles inflow/outflow self-similar solutions studied in the context of the core collapse leading to star formation (e.g., see the

circulation region in Fig. 1 of Lery et al. 2002; see also Henriksen, R.N., & Valls-Gabaud 1995, and reference therein). We also note that our solution could be qualitatively similar to inflow-outflow circulation found in the simulations of the magnetized cloud contracting under self-gravity (Tomisaka 1998) and to the funnel-wall jet found in fully relativistic numerical simulations of accretion disks in the Kerr metric (De Villiers et al. 2004).

We finish with two remarks: (i) The inflow/outflow solution is relevant to several astrophysical problems where some of the magnetized collapsing gas may have very low angular momentum (e.g., star forming regions, the Galactic center and other supermassive BH environments where the BH is surrounded by the diffused gas and mass losing stars, some GBRs and supernovae where it is believed that the explosion is related to a collapse of a massive rotating stellar envelope). (ii) Although our physics, initial and boundary conditions are simple compared to those in real systems, our inflow/outflow solution is simple and probably robust, and will help to pinpoint the key elements of real jets/outflows from low l accretion flows.

ACKNOWLEDGMENTS: We thank Philp Armitage, Mitch Begelman, Roger Blandford, Scott Kenyon, Tom Gardiner, Bohdan Paczyński, Jim Stone, and Dimitri Uzdensky for useful discussions. We also thank an anonymous referee for useful comments that helped us clarify our presentation. We acknowledge support from NASA under ATP grant NNG05GB68G and support provided by NASA through grant HST-AR-10305.05-A from the Space Telescope Science Institute, which is operated by the Association of Universities for Research in Astronomy, Inc., under NASA contract NAS5-26555.

REFERENCES

- Blandford, R.D., & Payne D.G. 1982, MNRAS, 199, 883
- Blandford, R.D., *Active Galactic Nuclei* (Eds R. Blandford, H. Netzer & L. Woltjer), Berlin: Springer 1990
- Balbus, S. A., & Hawley, J. F. 2002, ApJ, 573, 738
- De Villiers, J.-P., Hawley J.F., Krolik J.H., Hirose S. 2004, ApJ, in press (astro-ph/0407092)
- Henriksen, R.N., & Valls-Gabaud, D. 1994, MNRAS, 266, 681
- Lery, T., Henriksen, R.N., Fiege, J.D., Ray, T.P, Frank, A., & Bacciotti, F. 2002, A&A, 387, 187
- Kato, Y., Mineshige, S., & Shibata, K. 2004, ApJ, 605, 307

- McKinney, J.C., & Gammie, C.F. 2004, ApJ, 611, 977
- Mizuno, Y., Yamada, S., Koide, S., & Shibata, K. 2004, ApJ, 606, 395
- Paczyński, B., & Wiita, P. J. 1980, A&A, 88, 23
- Proga, D., & Begelman, M.C. 2003 ApJ, 582, 69 (PB03a)
- Proga, D., & Begelman, M.C. 2003 ApJ, 592, 767 (PB03b)
- Proga, D., MacFadyen, A.I., Armitage, P.J., & Begelman, M.C. 2003, ApJ, 599, L5
- Spruit, H. C. 1996, in *Evolutionary Processes in Binary Stars*, ed. R. A. M. J. Wijers, M. B. Davies, & C. A. Tout (Dordrecht: Kluwer), 249
- Stone, J.M., & Norman, M.L. 1994, ApJ, 433, 746
- Stone, J.M., & Norman, M.L. 1992a, ApJS, 80, 753
- Stone, J.M., & Norman, M.L. 1992b, ApJS, 80, 791
- Tomisaka K. 1998, ApJ, 502, L167
- Uchida, Y., & Schibata K. 1985, PASJ, 37, 515

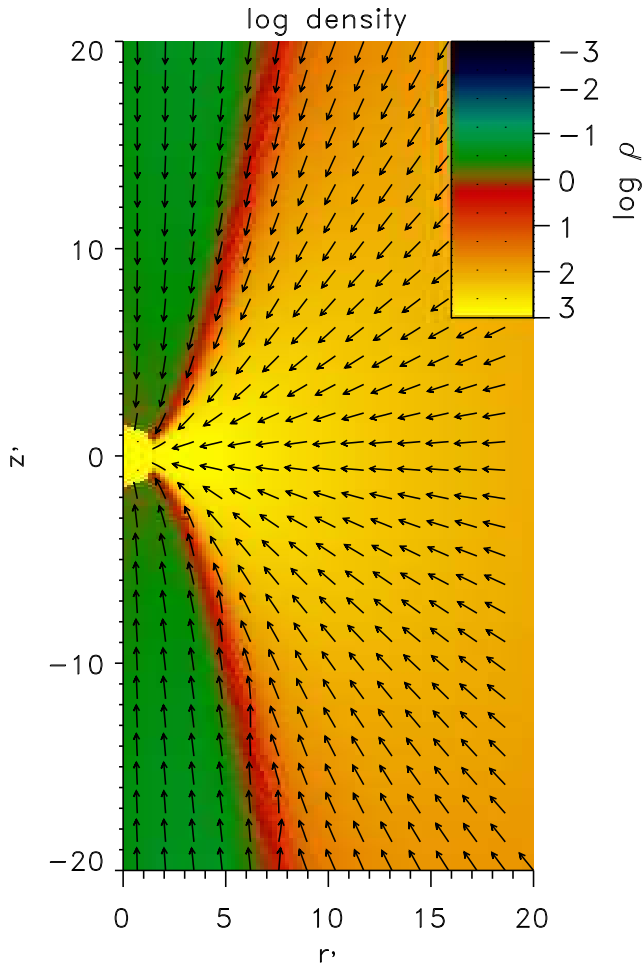


Fig. 1.— A map of logarithmic density overplotted with the direction of the poloidal velocity for model A (a zero magnetic field case).

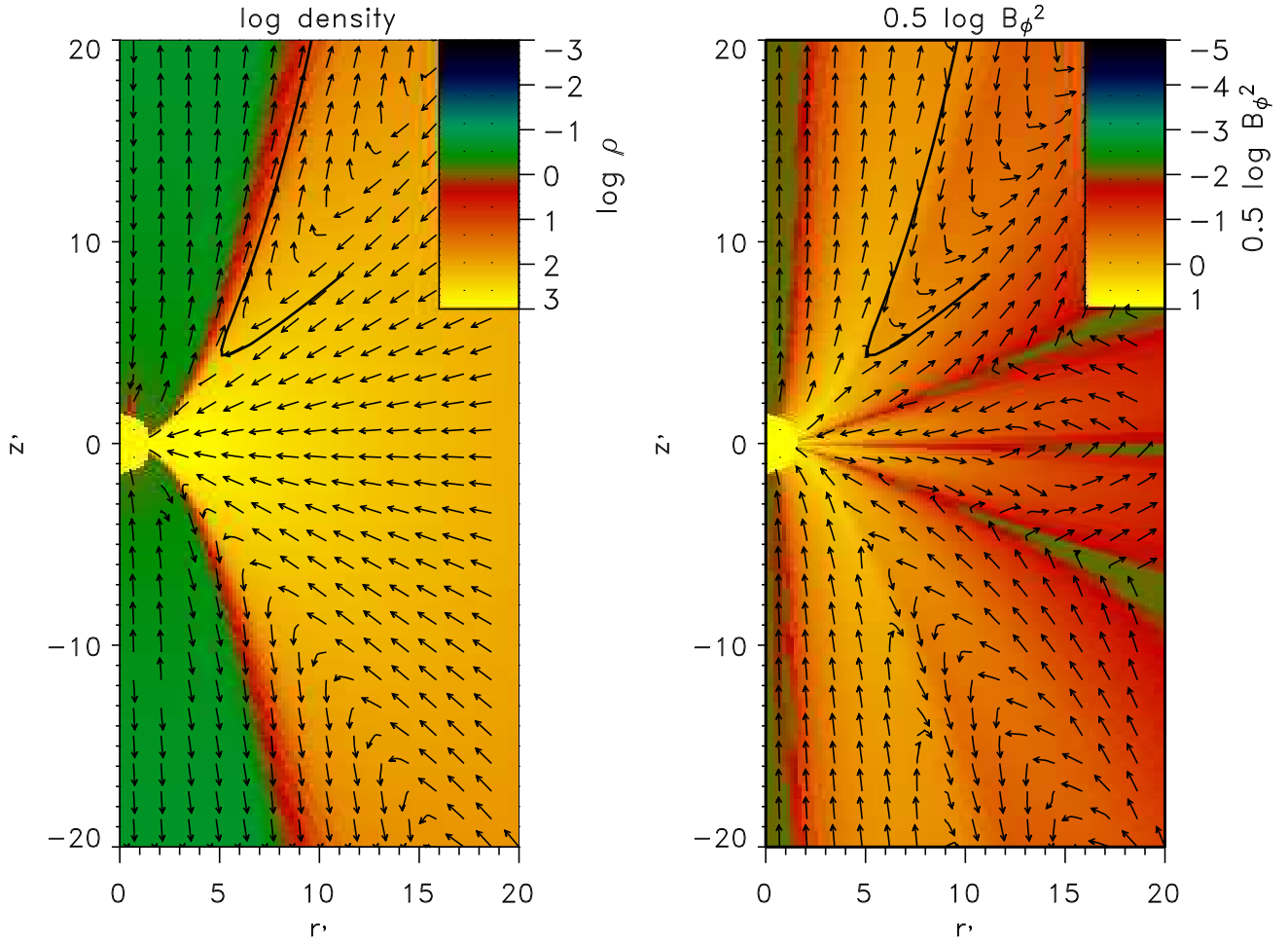


Fig. 2.— Maps of logarithmic density (left panel) and toroidal magnetic field (right panel) overplotted with an example of a streamline corresponding to an inflow/outflow for model B (a non-zero magnetic field case). The maps are also overplotted with the direction of the poloidal velocity and the direction of the poloidal field (the left and right panels, respectively).

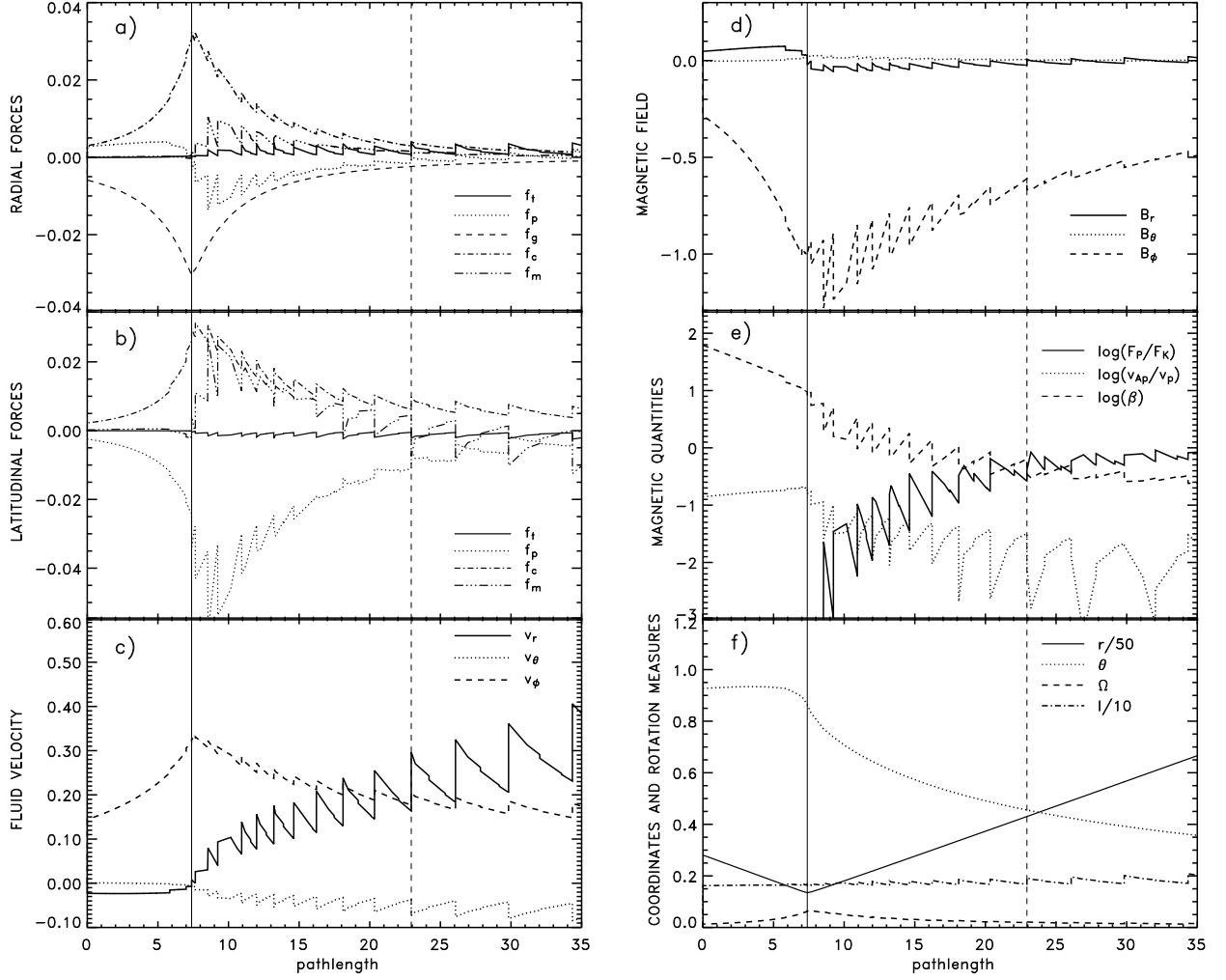


Fig. 3.— *From top to bottom:* The dominant forces in the radial and latitudinal directions (a and b panels, respectively) along the streamline presented in Fig. 2. The fluid and magnetic properties as a function of the pathlength along the streamline (c-f panels). For details see the labels and the main text. Note that the specific angular momentum, l is reduced by a factor of 10 while the radius along the stream line is reduced by a factor of 50 (dot-dashed line and solid line in panel f, respectively). The solid vertical lines in all panels correspond to the location where the flow reaches the stagnation point (the minimum radius along the streamline). The dashed vertical lines in all panels correspond to the location where the radial component of the magnetic field changes sign and indicates the location where the magnetic field associated with the bipolar outflow is advected into the grid cell with a much stronger, oppositely oriented magnetic field associated with the polar funnel.